HHS Public Access

Author manuscript

J Magn Reson. Author manuscript; available in PMC 2019 November 01.

Published in final edited form as:

J Magn Reson. 2018 November ; 296: 79–84. doi:10.1016/j.jmr.2018.09.001.

Capturing exchange using periodic radiofrequency irradiation

Timo Liimatainen[1,2,*], **Hanne Laakso**[3], **Djaudat Idiyatullin**[4], **Silvia Mangia**[4], **Shalom Michaeli**[4]

[1]Research Unit of Medical Imaging, Physics and Technology, University of Oulu, Oulu, Finland [2]Department of Diagnostic Radiology, Oulu University Hospital, Oulu, Finland [3]A.I.Virtanen Institute for Molecular Sciences, University of Eastern Finland, Kuopio, Finland [4]Center for Magnetic Resonance Research, University of Minnesota, Minneapolis, MN, USA

Abstract

The dynamics of spin system coupled by chemical exchange between two sites with different chemical shifts during periodic radiofrequency (RF) irradiation was here investigated. When the instantaneous π-flip of effective frequency during the course of frequency sweep was applied, a significant increase of exchange-induced relaxation rate constants was observed for small tip angle of magnetization in the laboratory frame of reference. This increase of the rate constants corresponds to the side bands generated by the periodic irradiation during the RF pulses. The exchange - induced relaxation rate constants depend on the exchange conditions, the RF power and the irradiation period. The described phenomenon promises applications for studying protein dynamics and for generating exchange specific relaxation contrasts in MRI.

Keywords

Chemical Exchange; Bloch - McConnell equations; RAFFn; Periodic RF Irradiation

Introduction

Application of periodic radiofrequency (RF) irradiation to a spin systems coupled by chemical exchange is an unexplored strategy in NMR. Periodic Hamiltonian can influence spin system undergoing anisochronous exchange, i.e., exchange between spins with different chemical shifts, by significantly increasing the relaxation rate constants in correspondence to the side bands generated during the RF pulses. There has been a considerable interest in utilizing periodic irradiation for various purposes in NMR. One example of applying periodic pulses is the Delays Alternating with Notations for Tailored Excitation (DANTE), which is a composite pulse formed by a series of hard pulses with optimized phases producing a wide band excitation with low RF peak power [1]. DANTE pulses have recently been applied for short echo time imaging to produce a high bandwidth excitation with low power and thus take advantage of increased signal to noise ratio when the signal from the

[*]**Corresponding author** Timo Liimatainen, Research Unit of Medical Imaging, Physics and Technology, University of Oulu / Oulu University Hospital, P.O.Box 50, 70029 OYS, FINLAND, timo.liimatainen@oulu.fi.

side bands generated during periodic irradiation was used for image encoding [2]. Similarly, the idea of sideband excitation has been implemented also for zero echo time imaging (ZTE) [3]. Another example of the applications of periodic irradiation includes the generation of magnetization transfer in MRI by using sidebands produced by the RF pulses [4] and generating adiabatic decoupling sidebands [5].

Conventional continuous wave rotating frame spin lock $T_{1\rho}$ experiment is typically performed without or with one phase shift during an RF pulse applied on/off resonance with the typical pulse duration in the *ms* time scale. However, the influence of periodicity of RF irradiation on exchange-induced relaxation rate constants in the off-resonance $T_{1\rho}$ experiment has not been evaluated so far [6]. In adiabatic $T_{1\rho}$ and $T_{2\rho}$ measurements [7–9], the periodicity of irradiation takes place during the train of adiabatic full passage (AFP) pulses with the phases usually prescribed according to MLEV - 4 [9,10]. Same applies to $T_{1\rho}$ and $T_{2\rho}$ measured using gradient modulated low-power adiabatic pulses [11], and Relaxation Along Fictitious Field in the rotating frame of rank n (RAFFn) [12–15], where the periodic irradiation takes place during rotating frame measurements in the rotating frames of rank 1–5. Conventional magnetization transfer (MT) experiments are conducted using continuous wave technique with relatively low RF power and long pulses used for off-resonance irradiation [16]. In several studies, however, the continuous wave RF pulse is replaced by periodic irradiation to obtain MT weighting. One example is Z-spectroscopy with Alternating-Phase Irradiation (ZAPI) method [17], where periodic sinusoidal modulation of the RF irradiation is applied on-resonance. During ZAPI the sidebands are generated symmetrically to the on-resonance frequency, and the periodicity of RF irradiation could be tuned to generate sidebands which are positioned optimally off-resonance to induce MT.

In this work, we studied the influence of the periodicity of RF irradiation on exchange - induced relaxation. We calculated relaxation rate constants during periodic irradiation applied to two-pool spin system coupled by equilibrium exchange. We varied tip angle of magnetization, irradiation period, irradiation power, and the fundamental MR parameters of two exchanging sites, and conducted simulations using Bloch-McConnell formalism [12]. The results of our analysis demonstrated that independently of pulse modulation functions of the frequency swept pulses, similar side bands which originate from the refocusing of magnetization were formed. Tuning the irradiation period to the chemical shift differences between exchanging sites allows significantly increasing the exchange-induced relaxation rate constants. As an example, here we analyze relaxation rate constants induced by exchange during the RAFFn family of frequency swept pulses. However, our findings are valid in general for other frequency swept pulses having amplitude and frequency modulation functions different from RAFFn, e.g., RF pulses of the hyperbolic secant family [18], as long as the instantaneous flip of the effective frequency takes place during the course of the RF irradiation, and the tip angle of magnetization from laboratory z axis is small.

Theory

Modulation Functions of RAFFn

The modulation functions of the method inducing relaxations in high rotating frames of rank n and entitled Relaxation Along a Fictitious Fields in the rotating frame of rank n (RAFFn) were recently described [12]. Below, we briefly summarize the recently presented detailed description of RAFFn pulse modulation functions. For obtaining time-invariant and equal amplitudes and frequency components in the first rotating frame (n=1), the amplitude $\omega_1^{(1)}$ and frequency $\Delta\omega^{(1)}$ modulation functions in the first rotating frame of reference are defined as follows:

$$\omega_1^{(1)} = \tan\alpha_1 \omega_1^{max} \quad (1)$$

$$\Delta\omega^{(1)} = \omega_1^{max},$$

where ω_1^{max} is the peak RF amplitude in rad/s. The recursive relationship which was used for amplitude and frequency modulation of RAFFn for n > 1 based on *sine*/*cosine* functions are given by:

$$\omega_1^{(n)}\left(t\right) = \Delta\omega^{(n-1)}\left(t\right) sin\left(\int \omega_1^{(n-1)}(t)dt\right) \quad (2)$$

$$\Delta\omega^{(n)}\left(t\right) = \Delta\omega^{(n-1)}\left(t\right) cos\left(\int \omega_1^{(n-1)}(t)dt\right)$$

for n = 2, 4, 6, … and

$$\omega_1^{(n)}(t) = \omega_1^{(n-1)}(t) sin\left(\int \Delta\omega^{(n-1)}(t)dt\right) \quad (3)$$

$$\Delta\omega^{(n)}(t) = \omega_1^{(n-1)}(t) cos\left(\int \omega^{(n-1)}(t)dt\right)$$

for n = 3, 5, 7, … . The pulse duration (T_p) is calculated as $4\pi/\left(\sqrt{2}\omega_1^{max}\right)$. Each *sine*/*cosine* pulse consists of four RAFFn pulse elements treated according to a refocusing scheme as was described in [12,14]. The average flip angle during the pulse was estimated by calculating the flip angle of magnetization from the Z axis of the laboratory frame in each pulse point using Bloch equations and averaging the angle over the duration of the pulse.

Bloch-McConnell Formulation of the Relaxation During RAFFn

Relaxations during RF irradiation due to the dipolar interactions (like spins) and induced by anisochronous exchange between two pools A and B with different chemical shifts can be described using Bloch-McConnell equations written in the phase-modulated rotating frame [15,19]:

$$\frac{dM_Z^A(t)}{dt} = \frac{M_0^A - M_Z^A(t)}{T_{1A}} - k_{ex}^{AB} M_Z^A(t) + k_{ex}^{BA} M_Z^B(t) + \omega_1 \sin(\varphi) M_X^A(t) - \omega_1 \cos(\varphi) M_Y^A(t)$$

$$\frac{dM_Z^B(t)}{dt} = \frac{M_0^B - M_Z^B(t)}{T_{1B}} - k_{ex}^{BA} M_Z^B(t) + k_{ex}^{AB} M_Z^A(t) + \omega_1 \sin(\varphi) M_X^B(t) - \omega_1 \cos(\varphi) M_Y^B(t)$$

$$\frac{dM_X^A(t)}{dt} = \frac{M_X^A(t)}{T_{2A}} - k_{ex}^{AB} M_X^A(t) + k_{ex}^{BA} M_X^B(t) - \Delta_A M_Y^A(t) - \omega_1 \sin(\varphi) M_Z^A(t)$$

$$\frac{dM_X^B(t)}{dt} = \frac{M_X^B(t)}{T_{2B}} - k_{ex}^{BA} M_X^B(t) + k_{ex}^{AB} M_X^A(t) - \Delta_B M_Y^B(t) - \omega_1 \sin(\varphi) M_Z^B(t)$$

$$\frac{dM_Y^A(t)}{dt} = \frac{M_Y^A(t)}{T_{2A}} - k_{ex}^{AB} M_Y^A(t) + k_{ex}^{BA} M_Y^B(t) - \Delta_A M_X^A(t) - \omega_1 \cos(\varphi) M_Z^A(t)$$

$$\frac{dM_Y^B(t)}{dt} = \frac{M_Y^B(t)}{T_{2B}} - k_{ex}^{BA} M_Y^B(t) + k_{ex}^{AB} M_Y^A(t) - \Delta_B M_X^B(t) - \omega_1 \cos(\varphi) M_Z^B(t) \quad (4),$$

where $\Delta_{A,B}$ are the chemical shifts in rad/s of exchanging groups A and B, respectively ($\delta\omega = |\Delta_A - \Delta_B|$), $k_{ex}^{AB} = P_B/\tau_{ex}$ and $k_{ex}^{BA} = P_A/\tau_{ex}$ are the exchange rate constants for exchanging site populations P_A and P_B, and $T_{1,2,A,B}=1/R_{1,2,A,B}$ are the relaxation time constants at sites A and B, respectively. The longitudinal R_1 and transverse R_2 free precession relaxation rate constants were calculated considering dipolar interactions between isolated identical spins:

$$R_1 = \frac{3}{10} b^2 \left(\frac{\tau_c}{1 + \tau_c^2 \omega_0^2} + \frac{4\tau_c}{1 + 4\tau_c^2 \omega_0^2} \right) \quad (5)$$

and

$$R_2 = \frac{3}{20} b^2 \left(3\tau_c + \frac{5\tau_c}{1+\tau_c^2\omega_0^2} + \frac{2\tau_c}{1+4\tau_c^2\omega_0^2} \right), \quad (6)$$

where τ_c is the rotational correlation time, ω_0 is the Larmor precession frequency, b = $-\mu_0\hbar\gamma^3/(4\pi r^3)$b=$-\mu_0\hbar\gamma^2/(4\pi r^3)$,$\mu_0$ is vacuum permeability, $\hbar$ is Planc's constant, γ is gyromagnetic ratio, and r is a hydrodynamic radius, similarly to what was used in [15]. The simulations of the two-site exchange were carried out using full Eq. 4. For all simulations, the calculations were performed with R_1 and R_2 obtained using Eq. 5 and 6 with τ_c = $2\cdot10^{-12}$ s for both sites A and B. The decay of **M** (**M**$_0$=[0 0 1]) during the pulse was estimated by solving partial differential equation (Eq. [4]) using variable step Runge-Kutta numerical method. Simulations were repeated for initially inverted magnetization **M**$_0$=[0 0 –1] including steady state formation. Because RAFFn pulses operate in the positive hemisphere, the application of RAFFn pulse train lead to a formation of the steady state when the magnetization is initially not perturbed [12,14,15]. We have demonstrated that the combined analysis of the SI evolution from positive +z and negative −z axes is essential for the accurate estimation of the relaxation rate constants during RAFFn [14]. This approach was previously described in details [14], and was shown to facilitate the analysis of the relaxations during RAFFn pulses [12,14,15].

Methods

Bloch-McConnell Simulations

All simulations were conducted using full set of two-pool Bloch-McConnell equations [4]. The T_1 and T_2 of the pools were calculated using the model of dipolar interaction between isolated spins using τ_c of $76\cdot10^{-12}$ s in equations (5) and (6). Simulations were performed for water at main magnetic field of 9.4 T with ^{1}H gyromagnetic ratio of 42.576 MHz/T, Planck's constant of $1.054571628\cdot10^{-34}$ Js, hydrodynamic radius of $158\cdot10^{-12}$ m [20], and permeability of vacuum of $4\pi\cdot10^{-7}$. The T_1 and T_2 were identical for both pools. Spin populations of the pools were set to P_A = 0.1 and P_B = 1-P_A and τ_{ex} was let to vary. Coalesced exchange peak was assumed so that off-resonance for spin pool A was $\Delta_A = 2\pi$ $P_B\cdot$[0 6 12… 3000] rad/s, and similarly for $\Delta_B = -2\pi$ $P_A\cdot$[0 6 12… 3000] rad/s. In RAFFn n was between 1 and 5, and if not otherwise stated, α_1 is 45° and $\omega_1^{max} = 2\pi\cdot625$ rad/s, if not otherwise stated. When ω_1^{max} is set in Eq. 1, the maximum amplitude of RAFFn pulse decreases with increasing n and is dependent on α_1. The actual maximum amplitude of RAFFn pulses are stated in the Figure legends. The number of points in waveform with refocusing scheme $PP_\pi{}^{-1}P_\pi P^{-1}$ [14] was 128, the refocused pulse duration $T_p = 4\pi/(\sqrt{2}\omega_1^{max})$ giving 18 μs time increment between simulation points. 64 pulses were added into pulse train resulting up to 144 ms long irradiation. Waveforms and refocusing scheme were created by equations written earlier [12,15]. Simulation of evolution of magnetization was done in Matlab (Mathworks Inc.) by solving Bloch McConnell equations by numerical partial differential equation solver (ode45, Matlab R2015a) time point-by-time

point fashion. The solver calculated the evolution of magnetization in several variable size sub-points between the points giving an extra confidence for magnetization evolution.

The time points 0 and 32 points evenly distributed within 144 ms were used to calculate relaxation rates from the simulated z-magnetizations. The z-magnetizations from both pools were summed up. Exponential decay taking into account steady state formation [14] was fitted to data points by using non-linear least square fitting routine if not another wise stated.

Results and Discussion

Simulations were conducted to evaluate the effect of periodic irradiation on exchanging two pool spin system. To demonstrate the effect of RF-pulse waveform on the relaxation rates over the range of different chemical shifts, frequency swept RF pulses with different amplitude and phase modulations were used. For the purpose of comparison, the average flip angle of the pulses were matched close to 5°. Notably, for all amplitude and phase modulation functions used for the calculations, an increase of the relaxation rate constants was found at the same chemical shift differences $\delta\omega$, and appeared in the shapes of well-defined peaks (Figure 1). The relaxation rate at $\delta\omega$=1500 Hz increased gradually from 10.9 s^{-1} with RAFF1 to 13.7 s^{-1} with RAFF5. The full-width-half-maximum (FWHM) of the relaxation rate peak increased from 52 Hz with RAFF1 to 173 Hz with RAFF5. An increase of relaxation rate constant with RAFF5 at $\delta\omega \approx 1500$ Hz can be explained by different contributions of the $T_{1\rho}$ and $T_{2\rho}$ relaxation channels, which were shown to provide different weightings in RAFFn [12]. These contributions vary with the tip angle of magnetization relatively to z axis of the laboratory frame. More complex amplitude and phase modulation functions of RAFF5 as compared to RAFF1 are responsible for the gradual increase of FWHM from RAFF1 to RAFF5. The analyses of the signal decay were based on single exponential fitting, which described sufficiently well the magnetization decay. The slight oscillations were observed when the relaxation reached their maximal values which corresponded to the peaks of the rate constants. Although this is the deviation from monoexponentiality, due to its minor oscillatory behavior the signal still was treated using monoexponential approximation.

The dependencies of the exchange induced relaxation rate constants on chemical shift difference for several exchange correlation times are shown in Figure 2. The simulation demonstrates that maximal relaxation effect of periodic irradiation on exchanging system is achieved for relatively slow correlation times (i.e, 10 and 100 ms) for the used pulse sequence settings. The increase of the rate constants is observed when the system moves to the fast exchange regime, as it could be seen for the case of τ_{ex}= 1 ms, with the further broadening of the side bands 300–700 Hz.

The simulation of RAFF1 with different α_1 angles demonstrates that the increase of the relaxation rate constants in correspondence of the side bands of the pulse occurs when magnetization is close to z-axis, i.e. when α_1 is small (Figure 3). The relaxation is boosted by ratio over 2 when chemical shift $\delta\omega$ between pools A and B is suitable for spin interaction in this case. This simulation differs from conventional off-resonance spin-lock $T_{1\rho}$ simulation by the fact that magnetization starts from z-axis, precesses around the

effective field and, due to refocusing, returns back to z-axis. When α_1 increases, the ratio of $T_{2\rho}$ over the $T_{1\rho}$ also increases being almost solely $T_{2\rho}$ for $\alpha = 85°$. For $\alpha > 45°$ the side bands were not observed (Figure 3). Interestingly, when similar simulation is done for RAFF2 with the same α_1, the results of the calculations with $\alpha = 5°$ and $\alpha = 85°$ are almost identical, which can be explained by the similarity of the $T_{1\rho}^{(n)}$ and $T_{2\rho}^{(n)}$ contributions in the rotating frame of rank (n-1). Another similarity is that magnetization is close to z-axis of the laboratory frame in both cases.

The analysis of the different durations of refocusing periods demonstrate that longer refocusing period leads to the relaxation rate peaks to move towards smaller $\delta\omega$ values (Figure 4). The pulse length T_p is controlled by length factor (LF), which at the same time controls the refocusing time. The peaks of the rate constants correspond to $1/T_p$, i.e. for pulse length factor (LF) =1, to 2.23 ms, and similarly for the other LFs. Another interesting observation is an increase of relaxation rate constants with the increase of RF power (Figure 5). Increase of the RAFF2 peak power without changing refocusing time leads to an increase of the average flip angle of **M**. Noticeably, the locations of the side bands are independent of pulse power, however higher power settings lead to an increase of the relaxation rate constants (Figure 5).

The contour plot of the relaxation rate constants during RAFF4 for different chemical shift differences and exchange correlation times is shown in Figure 6. It can be seen, that the increase of the exchange induced relaxation rate constants corresponds well with the side bands of the pulses when the instantaneous flip of the effective frequency occurs. Moreover, the enhanced rate constants at the side bands is observed for slow-to-intermediate exchange regimes, whereas when the system moves towards fast exchange limit, relaxation becomes very fast and enhancement at the side bands is not discernible any longer. For comparison, the simulatiotions of exchange induced relaxations during adiabatic $T_{1\rho}$, $T_{2\rho}$ [7–9,21] and continuous wave spin lock $T_{1\rho}$ experiments are shown (Figure 7). Here, an increase of the relaxation rate constants which takes place during the P-packed RAFFn pulses, was not noticed. This further confirms necessity of the instantaneous flip of the effective frequency, i.e., change of the direction of the frequency sweep during the course of the RF pulse, to enable an enhancement of exchange induced rate constants which becomes discernible for relatively small tip angle of magnetization.

To summarize, we demonstrate here that instantaneous flip of the effective field during rotating frame experiments could lead to an increase of the exchange-induced relaxation rate constant. The detailed description of this phenomenon is described for the family of RAFFn pulses. This phenomenon was overlooked in NMR so far, and could find important applications for studying exchanging systems in protein dynamics, and for detection of exchange – related processes in living samples. This methodology could serve as a sensitive non-invasive MRI tool for generating exchange-induced tissue contrast when selectively tuning to the chemical shifts of interest, and may compliment and even over perform established MRI modalities such as T_2- and T_1- weighted methods, other rotating frame and Chemical Shift Saturation Transfer (CEST) techniques.

Conclusions

Numerical analysis of exchange-induced relaxation for two-site exchange during periodic irradiation demonstrate an increase of the relaxation rate constants which corresponds to the off-resonance side bands, and depends on the repetition rate of irradiation and the tip angle of magnetization. Simulations show that periodic irradiation produces sidebands in the chemical shift domain when the **M** remains only in one hemisphere, and the tip angle of **M** is relatively small, $\alpha < 45°$. Furthermore, Bloch-McConnell simulation of RF pulses with different modulation functions of the RAFFn family demonstrate that for fixed average flip angles the position of side bands in chemical shift domain remains constant, independently from the pulse modulation functions. Moreover, the pulse amplitude does not influence the location of the sidebands while increasing the overall relaxation rate constants. This methodology could serve as a sensitive tool for investigating exchange processes in both protein dynamic and non-invasive MRI applications when selectively tuning the side bands created by the periodicity of the frequency irradiation to the chemical shift of interest, and may compliment and even over-perform other established modalities such as Chemical Shift Saturation Transfer (CEST) [22]. The experimental verification is the subject of future work.

Acknowledgements

The authors would like to thank following funding sources for financial support Instrumentarium Science Foundation (HL), EU H2020 Marie Skłodowska RISE project #691110 (MICROBRADAM), Academy of Finland grants #275453 and #298007, NIH grants U01-NS103569, 1R01AG055591, BTRC, P41 EB015894, P30 NS057091. SM was supported by Fulbright-Saastamoinen Foundation Grant in Health and Environmental Science.

References

[1]. Bodenhausen G, Freeman R, Morris GA, A simple pulse sequence for selective excitation in Fourier transform NMR. J Magn Reson, 23 (1976) 171–175.

[2]. Idiyatullin D, Corum CA, Garwood M, Multi-Band-SWIFT. J Magn Reson, 251 (2015) 19–25. [PubMed: 25557859]

[3]. Brunner DO, Pavan M, Dietrich B, Rothmund D, Heller A, Pruessmann KP, Sideband Excitation for Concurrent RF Transmission and Reception, Proc Int Soc Magn Reson Med, (2011) 625.

[4]. Portnoy S, Stanisz GJ, Modeling pulsed magnetization transfer. Magn Reson Med, 58 (2007) 144–155. [PubMed: 17659607]

[5]. Zhang S, Gorenstein DG, Adiabatic decoupling sidebands. J Magn Reson, 144 (2000) 316–321. [PubMed: 10828199]

[6]. Podkorytov IS, Skrynnikov NR, Microsecond time-scale dynamics from relaxation in the rotating frame: experiments using spin lock with alternating phase. J Magn Reson, 169 (2004) 164–173. [PubMed: 15183365]

[7]. Michaeli S, Sorce D, Idiyatullin D, Ugurbil K, Garwood M, Transverse relaxation in the rotating frame induced by chemical exchange. J Magn Reson, 169 (2004) 293–299. [PubMed: 15261625]

[8]. Michaeli S, Sorce D, Springer C, Ugurbil K, Garwood M, $T_{1\rho}$ MRI contrast in the human brain: modulation of the longitudinal rotating frame relaxation shutter-speed during an adiabatic RF pulse. J Magn Reson, 181 (2006) 138–150.

[9]. Michaeli S, Sorce D, Garwood M, T2ρ and T1ρ Adiabatic Relaxations and Contrasts. Current Analytical Chemistry, 4 (2008) 8–25.

[10]. Levitt M, Freeman R, Frenkel T, Broadband heteronuclear decoupling. J Magn Reson, 47 (1982) 328–330.

[11]. Andronesi OC, Ramadan S, Ratai EM, Jennings D, Mountford CE, Sorensen AG, Spectroscopic imaging with improved gradient modulated constant adiabaticity pulses on high-field clinical scanners. J Magn Reson, 203 (2010) 283–293. [PubMed: 20163975]

[12]. Liimatainen T, Hakkarainen H, Mangia S, Huttunen JM, Storino C, Idiyatullin D, Sorce D, Garwood M, Michaeli S, MRI contrasts in high rank rotating frames. Magn Reson Med, 73 (2015) 254–262. [PubMed: 24523028]

[13]. Hakkarainen H, Sierra A, Mangia S, Garwood M, Michaeli S, Gröhn O, Liimatainen T, MRI relaxation in the presence of fictitious fields correlates with myelin content in normal rat brain. Magn Reson Med, 75 (2016) 161–168. [PubMed: 25648507]

[14]. Liimatainen T, Sorce DJ, Connell R, Garwood M, Michaeli S, MRI Contrast from Relaxation Along a Fictitious Field (RAFF). Magn Reson Med, 64 (2010) 983–994. [PubMed: 20740665]

[15]. Liimatainen T, Mangia S, Ling W, Ellermann J, Sorce D, Garwood M, Michaeli S, Relaxation Dispersion in MRI Induced By Fictitious Magnetic Fields. J Magn Reson, 209 (2011) 269–276. [PubMed: 21334231]

[16]. Wolff SD, Balaban RS, Magnetization transfer contrast (MTC) and tissue water proton relaxation in vivo. Magn Reson Med, 10 (1989) 135–144. [PubMed: 2547135]

[17]. Närväinen J, Hubbard PL, Kauppinen RA, Morris GA, Z-spectroscopy with Alternating-Phase Irradiation. J Magn Reson, 207 (2010) 242–250. [PubMed: 20920868]

[18]. Garwood M, DelaBarre L, The return of the frequency sweep: designing adiabatic pulses for contemporary NMR. J Magn Reson, 153 (2001) 155–177. [PubMed: 11740891]

[19]. Mc Connell HM, Reaction Rates by Nuclear Magnetic Resonance. J Chem Phys, 28 (1958) 430–431.

[20]. Carrington A, McLachlan AD. Introduction to Magnetic Resonance with Applications to Chemistry and Chemical Physics, Harper 1967.

[21]. Mangia S, Liimatainen T, Garwood M, Michaeli S, Rotating frame relaxation during adiabatic pulses vs. conventional spin lock: simulations and experimental results at 4 T. Magn Reson Imaging, 27 (2009) 1074–1087. [PubMed: 19559559]

[22]. Walker-Samuel S, Ramasawmy R, Torrealdea F, Rega M, Rajkumar V, Johnson SP, Richardson S, Goncalves M, Parkes HG, Arstad E, Thomas DL, Pedley RB, Lythgoe MF, Golay X, In vivo imaging of glucose uptake and metabolism in tumors. Nat Med, 19 (2013) 1067–1072. [PubMed: 23832090]

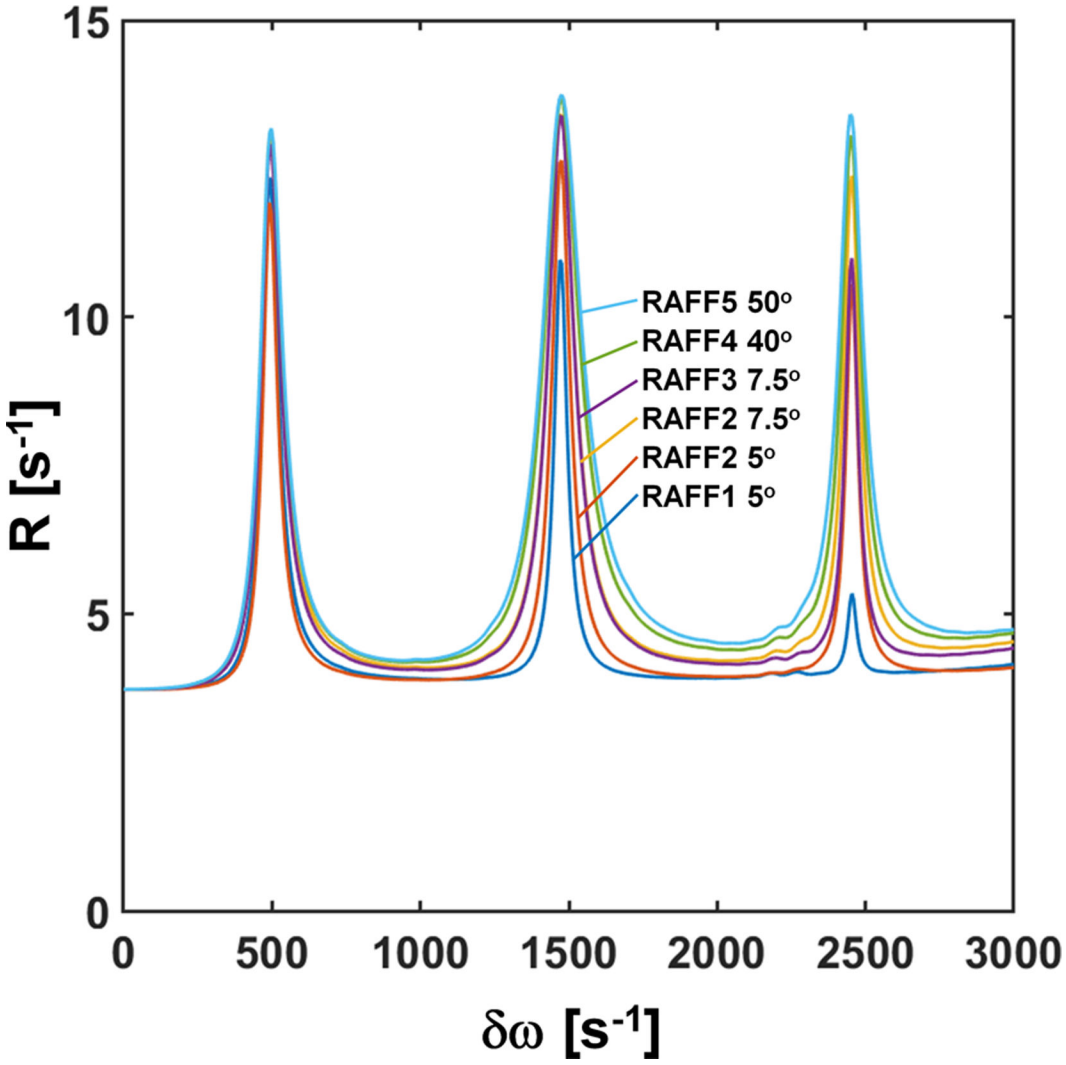

Figure 1.

Exchange-induced relaxation rate constant during periodic irradiation of RAFFn, where n = 1–5. Average flip angle during the pulses is adjusted close to 5° leading to following actual pulse powers (RAFF1 5.04° 55 Hz, RAFF2 3.82° 125 Hz, RAFF2 5.75° 186 Hz, RAFF3 4.94° 150 Hz, RAFF4 4.92° 273 Hz, and RAFF5 4.86° 249 Hz) by altering α_1 in equation (1) for RAFF1–5. Note that RAFF2 is repeated with two different α_1. Exchange correlation times of 10 ms, P_A=0.1, and τ_c=76·10^{-12} s for both sites were used.

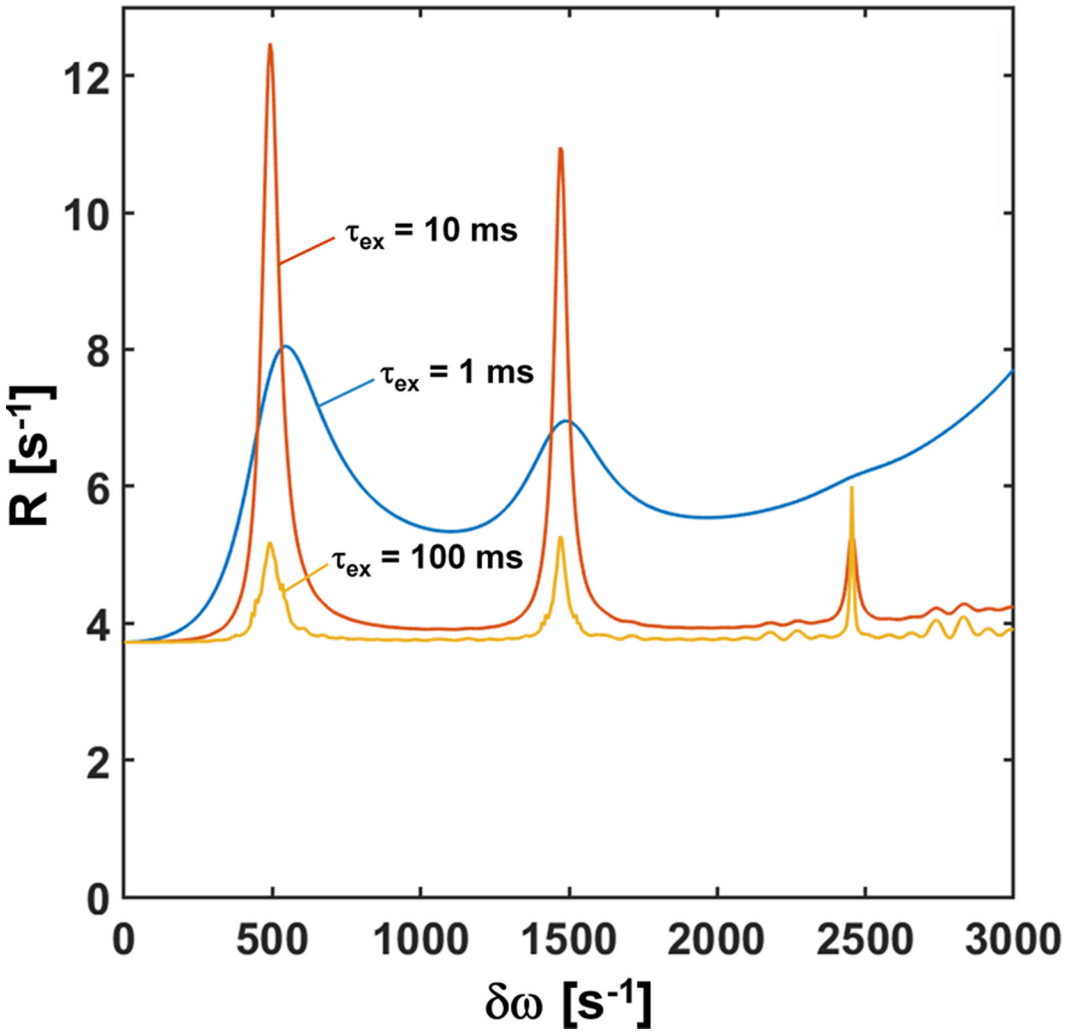

Figure 2.

Chemical exchange-induced relaxation rate constant's dependence on correlation time between the sites A and B. For simulations, amplitude and phase modulated RF waveform of RAFF1 pulse was used, RAFF1 pulse duration was 2.66 ms, ω_1^{max}= 625 Hz, α_1=5°, leading to actual pulse power of 55 Hz, P_A=0.1, and τ_c=76·10^{-12} s for both sites were used. Exchange correlation times were 1 ms, 10 ms and 100 ms as indicated on the plot.

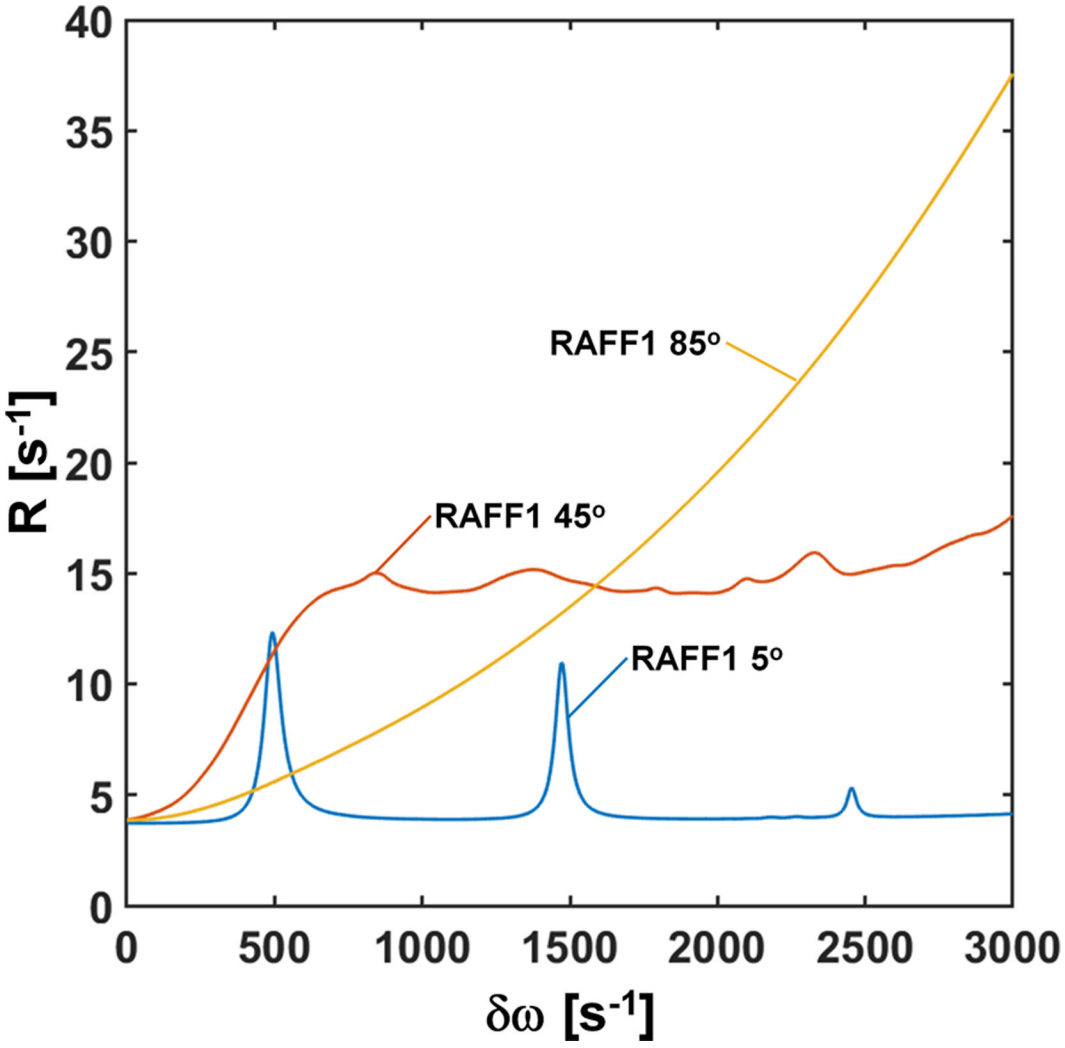

Figure 3.

Effect of α_1 for relaxation rate profile in periodic continuous wave irradiation. Note that increasing α_1 increases the average flip angle in RAFF1 and therefore RAFF1 $\alpha_1 = 5°$ (actual power 55 Hz) is more off-resonance $T_{1\rho}$ type measurement and RAFF1 $\alpha_1 = 85°$ (actual power 625 Hz) is more on-resonance $T_{2\rho}$ type measurement with refocusing.

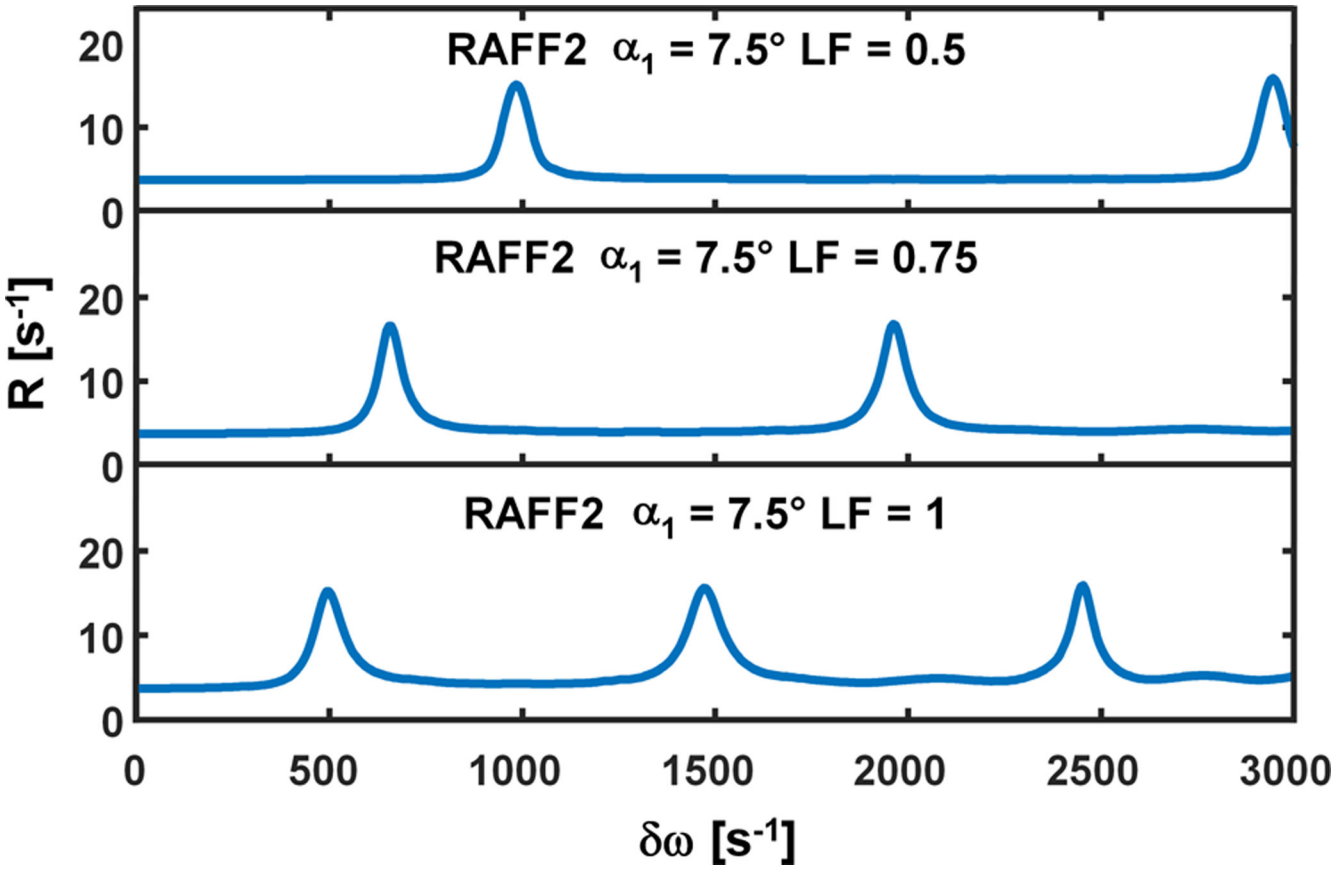

Figure 4.

Dependence of exchange-induced relaxation rate constants on the refocusing period of the irradiation. RAFF2 with $PP_{\pi}{}^{-1}P_{\pi}P^{-1}$ refocusing **top**: with length factor (LF) 0.5 resulting pulse duration of 1.1 ms and actual power of 97 Hz, **middle:** LF=0.75 resulting pulse duration of 1.7 ms and actual power of 142 Hz, and **bottom:** LF=1 to nominal RAFF2 pulse duration of 2.3 ms and actual power of 186 Hz. For simulations, exchange correlation time 10 ms, P_A=0.1, and τ_c=76·10^{-12} s for both sites were used.

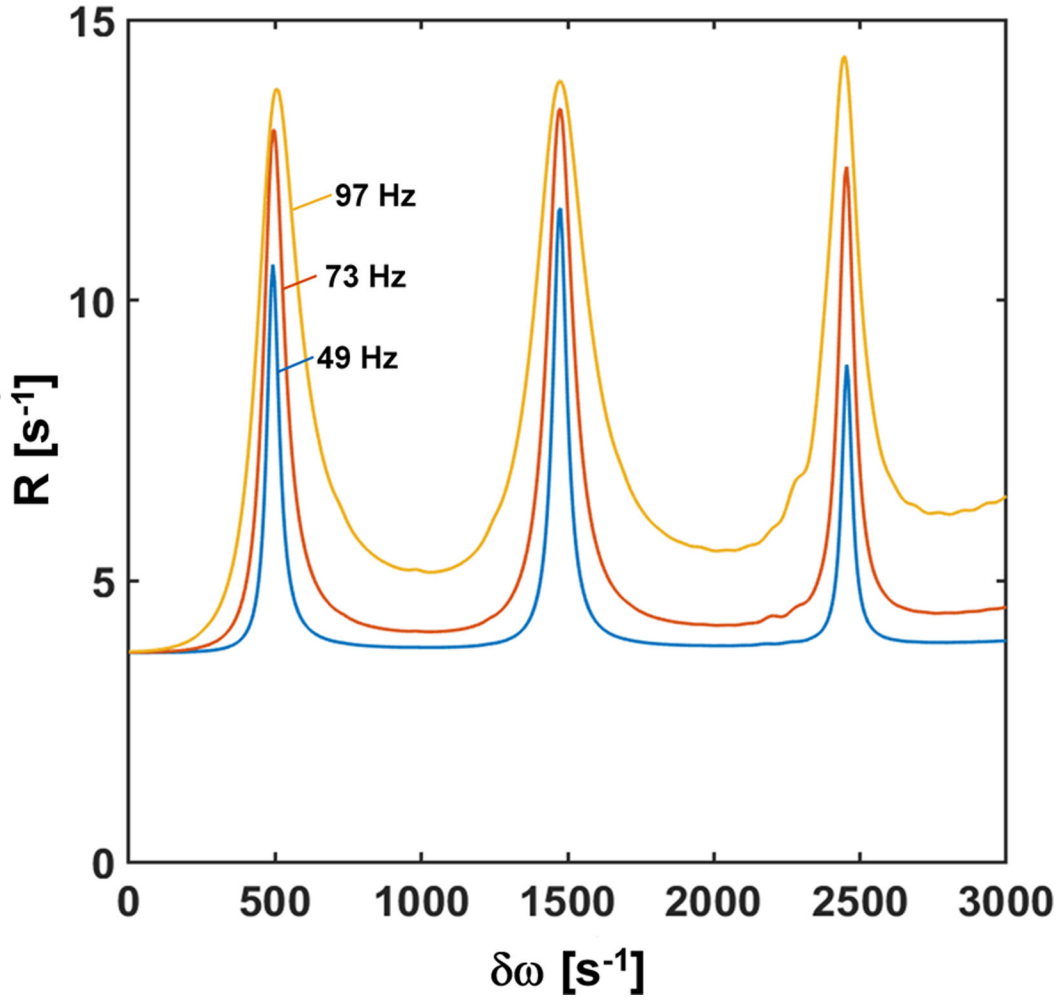

Figure 5.

Dependence of exchange-induced relaxation rate on RF power. RAFF2 $PP_{\pi}^{-1}P_{\pi}P^{-1}$ packets were used with refocusing period 2.3 ms, $\alpha_1 = 7.5°$, $\omega_1^{max} = 625$ Hz. The pulse amplitude was multiplied by 0.5, 0.75 or 1 leading to actual pulse powers of 49, 73 and 97 Hz. For simulations, exchange correlation time 10 ms, $P_A=0.1$, and $\tau_c=76\cdot10^{-12}$ s for both sites were used.

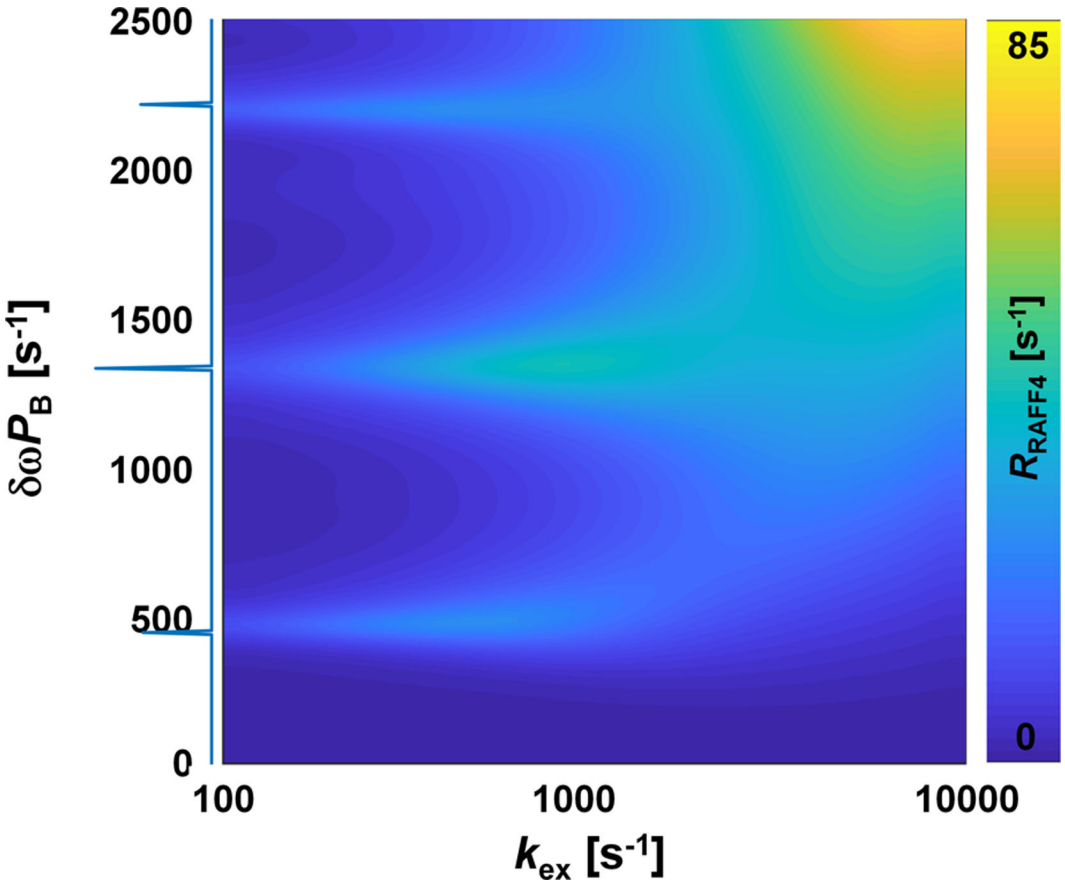

Figure 6.

Two dimensional plot of exchange-induced relaxation rate constant versus chemical shift differences between exchanging sites A and B. For the simulations RAFF4 45° pulses with $PP_{\pi}^{-1}P_{\pi}P^{-1}$ packets were used with refocusing period of 2.3 ms and with nominal ω_1^{max}= 625 Hz leading to actual pulse power of 140 Hz. k_{ex} values were logarithmically distributed between 100 and 10000 s^{-1} and 101 δω values were simulated between 0 and 3000 Hz with P_A=0.1, and τ_c=76·10^{-12} s for both sites. After simulation, relaxation rate data was interpolated to 1024 × 1024 image points with bicubic interpolation. On the left, fast Fourier transform of RAFF4 45° pulse train in the form $\omega_1^{max}(\cos(\varphi) + i\sin(\varphi))$ is shown in the frequency coordinates which is matched with the 2D plot.

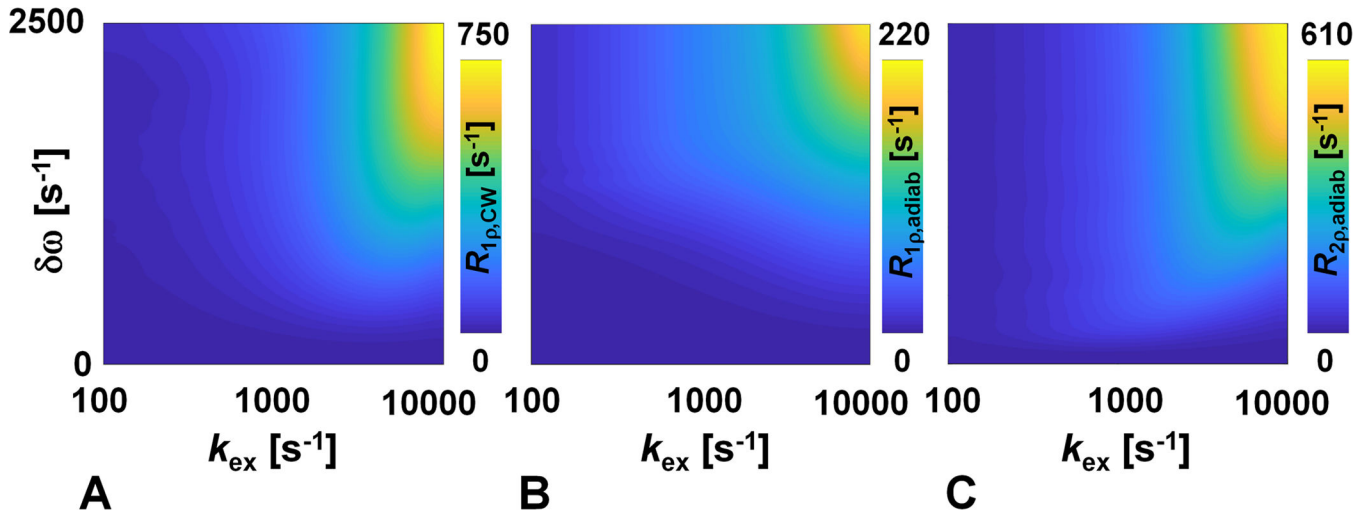

Figure 7.

Two dimensional plot of exchange-induced relaxation rate constant versus chemical shift differences between exchanging sites A and B. (A) continuous wave $T_{1\rho}$, (B) adiabatic $T_{1\rho}$ and (C) adiabatic $T_{2\rho}$ simulations. For the simulations Hyperbolic Secant continuous wave (CW) (A) and (HS) pulses (B and C) were used. Peak power ω_1^{max}= 625 Hz (A) and 2500 Hz (B and C). Adiabatic pulse duration T_p = 4 ms. Pulses were cycled according to MLEV-4 [10]. In adiabatic $T_{1\rho}$ magnetization was initially not perturbed, i.e., was along z'-axis of the first rotation frame. In adiabatic $T_{2\rho}$ magnetization is initially placed in the transverse plan. In all plots, k_{ex} values were logarithmically distributed between 100 and 10000 s^{-1} and 101 δω values were simulated between 0 and 3000 Hz with P_A=0.1, and τ_c=76·10^{-12} s for both sites. After simulation, relaxation rate data was interpolated to 1024 × 1024 image points with bicubic interpolation.